ARTICLE

Mechanical and Tribological Behavior of Graphene Oxide Supported Aramid Fiber Reinforced Epoxy Resin

Yuanyuan Feng[1], Bingli Pan[1,*], Hongyu Liu[1,2], Yuxuan Zhou[1], Xiaofan Ding[1] and Xinyu Yuan[1]

[1]School of Chemistry and Chemical Engineering, Henan University of Science and Technology, Luoyang, 471023, China

[2]Department of Polymer-Science and Technology, Jeonbuk National University, Jeonju, 54896, Republic of Korea

*Corresponding Author: Bingli Pan. Email: blpan@haust.edu.cn

ABSTRACT

In this paper, knitted aramid fiber (AF) was used as the support, and graphene oxide (GO) was loaded on the support by the polydopamine (PDA) method. Epoxy resin (EP) was poured to obtain composite materials. The tribological and mechanical properties of the composites were tested, and the wear surface of the composites was characterized by scanning electron microscopy (SEM) and three-dimensional morphology. The results show that knitted AF can markedly improve the mechanical properties of the composites. As a two-dimensional material, GO plays an effective lubrication role, and GO effectively enhances the tribological properties of the composites. AF can reduce the wear rate of composites and improve the tribological properties of composites. During the friction process, AF and GO play a synergistic role, which can form a friction transfer film between the matrix and the friction medium, thereby avoiding direct contact between the matrix and the friction medium and improving the tribological properties of the composites. EP/AF/PDA (Dopamine hydrochloride)/GO has the best modification effect on the tribological properties of the composites. Compared with the friction coefficient of pure EP, the friction coefficient of EP/AF/PDA/GO is reduced by 48.36%, and the volume wear rate is reduced by 96.99% compared with pure EP.

KEYWORDS

Aramid fiber; graphene oxide; epoxy resin; tribological behaviors

1 Introduction

Epoxy resin (EP) is widely used in aerospace, automotive, and mechanical equipment [1–3] in mining due to its excellent mechanical properties, thermal stability, superior electrical insulation, and chemical resistance [4], as well as ease of processing and low cost, with applications in coatings, composites [5], casting materials [6], adhesives [7], fire retardant material [8], and injection molding materials. However, its high brittleness [9] and high friction coefficient [10] have limited its widespread application. To address this issue, adding other materials (such as sponges, fibers, etc.) to EP materials to improve the performance of the obtained composite materials is widely used. Fibers such as aramid fiber (AF) [11–14], carbon fiber (CF) [15–17], and basalt fiber (BF) [18–20] have been introduced

into the epoxy resin to improve its performance. AF, in particular, is commonly used in polymer composites due to its low density, high specific strength, high specific modulus, and high-temperature resistance [21,22] developed aramid pulp/carbon fiber reinforced polybenzoxazine composites as high-performance friction materials with high thermal degradation temperature, glass transition temperature, and good wear resistance. Through the method of knitted aramid fiber, the fiber can form a support, so that it can play a greater role in the composite material [23,24].

To achieve the desired effect of fiber reinforcement, it is vital to improve the interactions between the matrix and the filler surface [25–28]. Therefore, methods for modifying the fiber surface have been developed, including surface etching [29], plasma processing [30], and coating [31,32], to improve the performance of the fiber/resin composite. Surface etching involves chemically etching the fiber surface, which affects the fiber's properties. Reference [33] used LiF/HCl solution etching Ti_3AlC_2 to synthesize $Ti_3C_2T_x$ MXene and it was utilized for surface modification of polyethylene (PE) fiber to form a stable absorptive buffer layer on the fiber interface. Inspired by the strong adhesion ability of polydopamine (PDA) originating from the mussel secretory gland, dopamine. Sun et al. [34] used a PDA coating quickly and uniformly formed on CF through the rapid synthesis under anoxic conditions by ultrasound, to change the interface of the composite. To improve the frictional properties of the composites, nanomaterials such as graphene oxide (GO) [35], carbon nanotubes (CNF) [19], and reduced graphene oxide (rGO) [36] are often added. Compared to CNF and rGO, GO contains carboxyl (-COOH), hydroxyl (-OH), and epoxy (-O-) functional groups [37], which can enhance the chemical interactions between the polymer matrix and the nanomaterials. Thus, GO can effectively improve the tribological properties of composites. Wang et al. designed a porous 3D graphene lubricant using polyurethane (PU) foam carrier, and then poured monomer-casting polyamide 6 (MCPA6) into the 3D graphene lubricant to prepare a self-lubricating composite material [38]. However, direct coating of GO on the fiber surface is challenging [39]. Feng et al. [40] adhered PDA-modified reduced graphene oxide (PDA-rGO) to the nickel foam skeleton; the self-polymerized PDA layer binds GO to the fiber through chemical interactions and improves the tribological properties of the composites [41]. According to published reports, there is no report on the use of polydopamine modification to load GO onto knitted aramid fibers to improve the properties of epoxy resin.

Based on the above survey, in this study, the tribological properties of EP were improved by incorporating a knitted aramid fiber/polydopamine/graphene oxide woven support framework into the EP matrix. AF can improve the mechanical properties of the matrix and reduce the volume wear rate. Coating the surface of AF by PDA can make the surface of AF load other substances. We selected GO as the modified material on account of GO was two-dimensional functional material with certain lubrication properties. The purpose of this study was to investigate the effect of PDA and GO on the properties of knitted aramid fiber composites, and to provide a basis for future research.

2 Experiments

2.1 Materials

The aramid fiber is from Dongguan Shenglan Rope Belt Weaving Co., Ltd. (Dongguan, China). Dopamine hydrochloride (PDA; $C_8H_{11}NO_2 \cdot HCl$) from Hefei BASF Biotechnology Co., Ltd. (Hefei, China). Tris (Tris; $NH_2C(CH_2OH)$) was purchased from Tianjin Deen Chemical Reagent Co., Ltd. (Tianjin, China). Graphite flakes (800 mesh), sulfuric acid (95%–98%), potassium permanganate were purchased from Qingdao Tianshengda Graphite Co., Ltd. (Qingdao, China), Luoyang Haohua Chemical Co., Ltd. (Luoyang, China), Tianjin Chemical Co., Ltd. (Tianjin, China). Hydrogen peroxide (30%), sodium hydroxide (analytically pure), sodium nitrate (analytically pure) and hydrochloric acid (37%) were all from Tianjin Damao Chemical Reagent Factory (Tianjin, China). E-44 epoxy resin and 650 curing agent (polyamide resin) are provided by Dingyuan Danbao Resin Co., Ltd. (Zhenjiang,

China). Unless otherwise stated, all chemical reagents and solvents are used as received without further purification.

2.2 Knitted AF Modified and Load GO

2.2.1 Preparation of PDA Modified Knitted AF

Aramid fabric with 30 mm × 30 mm aramid rope was knitted by hand knitting method. With 0.5 g dopamine hydrochloride, 0.3 g TRIS configuration solution 250 mL, with 10% HCl solution to adjust the solution pH = 8.5, get 2 g/L PDA solution. The treated aramid fabric was then placed in the solution for 24 h and continuously stirred. The soaked fabric was rinsed with distilled water for three times and dried at 60°C for 6 h to obtain AF/PDA.

2.2.2 Preparation of GO and AF/PDA Load GO

Graphene oxide was prepared by the improved Hummers method [42] and graphene oxide was prepared by ultrasonic method.

The GO solution was prepared according to the required graphene oxide concentration, and the AF/PDA fabric obtained in the previous step was placed in it, soaked for 24 h, and dried at 80°C for 10 h to obtain AF/PDA/GO.

2.3 Preparation of EP/AF/PDA/GO

Put the cleaned beaker on the balance, put it into the rotor, weigh a certain amount of epoxy resin, then add ethanol in proportion, stir it with a magnetic stirrer, and then weigh the polyamide resin in proportion, and stir it evenly. After ultrasonic defoaming for 30 min in an ultrasonic cleaner, it was poured into a mold with an AF/PDA/GO support skeleton, dried at 45°C for 4 h, and then placed for 2 d to solidify and demould. The preparation process of EP/AF/PDA/GO composites is shown in Fig. 1a.
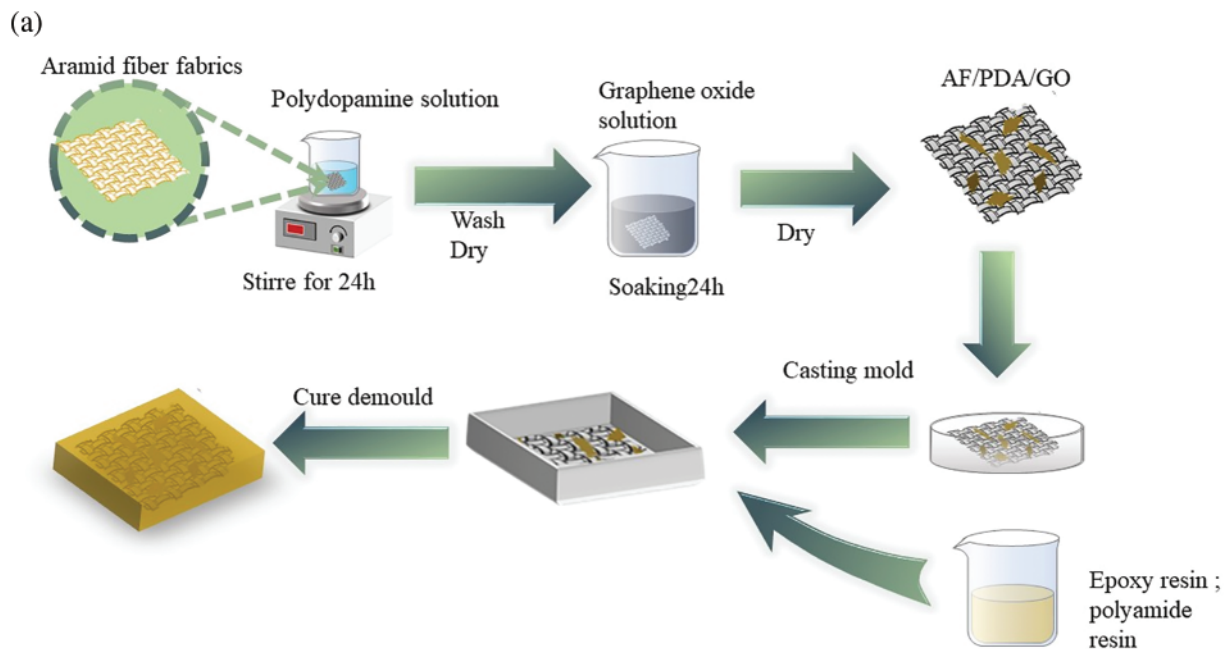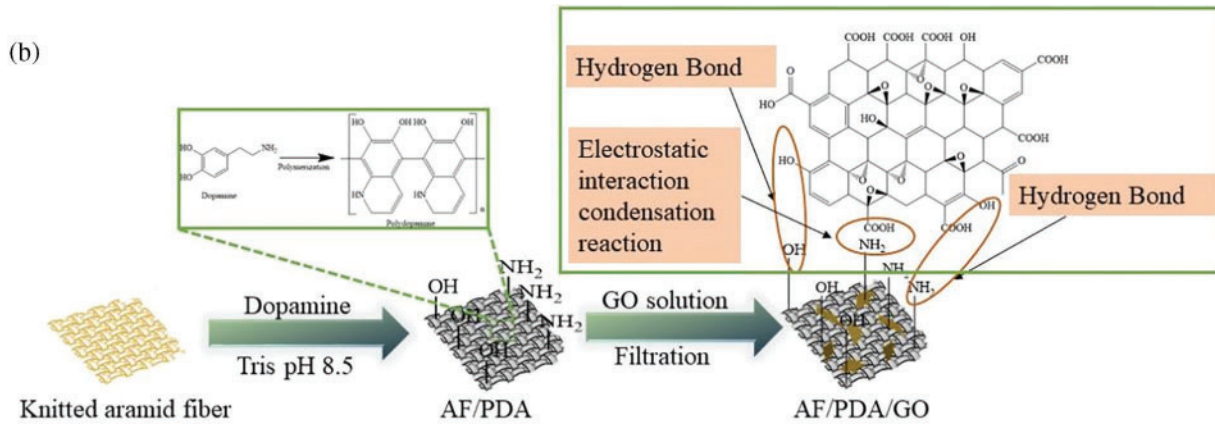

Figure 1: (Continued)

Figure 1: (a) Schematic diagram of EP/AF/PDA/GO composites preparation process, (b) Interaction mechanism between different components

2.4 Characterizations and Instruments

The worn surfaces of EP, EP/AF, EP/AF/PDA, EP/AF/PDA/GO composites were characterized by scanning electron microscopy (SEM, JSM-IT100, JEOL Inc., Tokyo, Japan). FTIR analysis was performed using an IRTracer-100 spectrometer (FTIR, Nicolet iS50, Thermo Scientific, Huntham, MA, USA) to characterize the composite and modified fiber groups in the range of 400–4000 cm^{-1}. The three-dimensional surface morphology of the wear track of EP composites was measured by scanning electron microscopy (SEM, JSM-IT100, JEOL Inc., Tokyo, Japan).

2.5 Mechanical and Tribological Tests

The hardness of the samples was tested by Shore hardness tester (LXD-D, Dongguan Three Measuring Tools Co., Ltd., Dongguan, China) according to GB 2411-80. Each sample was tested 5 times, and the average value was taken as the hardness. According to GB/T 1040, 224–228, the samples were made into dumbbell type, 3 in each group, a total of 4 groups. The tensile strength and modulus of EP and its composites were tested by electronic universal testing machine controlled by CMT4503 microcomputer (CMT4503, Master Industrial Systems Inc., Shenzhen, China), and the tensile speed was set to 2 mm/min. The tensile strength and modulus values are calculated according to the following equations:

$$\sigma = \frac{p}{b-h} \tag{1}$$

$$E = \frac{\Delta\sigma}{\Delta\varepsilon} \tag{2}$$

where σ (MPa) is the tensile strength, p(N) is the breakage load, b(mm) is the sample width, and h(mm) is the sample thickness; E is the tensile modulus, $\Delta\sigma$ indicates the increase in stress on the specimen, $\Delta\varepsilon$ is the strain of the tensile specimen.

According to the standard test method of GB 3960–1983, the friction and wear properties of EP composites were evaluated on MM-2HL ring block tester (MM-2HL, Jinan HengXu Testing Machine Technology Co., Ltd., Jinan, China). The sample size is 30 mm × 7 mm × 6 mm, and the dual material is carbon steel (45#) ring. Before the test, the surface of the dual material was polished with 1000# sandpaper and washed with ethanol. The friction test was carried out at room temperature. The normal load was 40 N and the sliding speed was 0.21 m/s. Three friction and wear tests were carried out on each sample. After the test, the wear volume ΔV(mm^3) of the specimen is calculated according to the

following formula [23]:

$$\Delta V = B \cdot \left[\frac{\pi R^2}{180} \cdot \arcsin\left(\frac{b}{2R}\right) - \frac{b}{2}\sqrt{R^2 - \frac{b^2}{4}} \right] \tag{3}$$

In the formula, B(mm) is the width of the specimen, R(mm) is the radius of the carbon steel ring, and b(mm) is the width of the wear scar. The specific wear rate W(mm³/Nm) was calculated according to the following formula:

$$W = \frac{\Delta V}{Ld} \tag{4}$$

In the formula, L(N) is the load and d(m) is the total sliding distance.

3 Result and Discussion

3.1 Microstructure of the AF with Different Surface Treatments

Fig. 1b shows the physical and chemical changes on the surface of AF. During the preparation process, the polydopamine coating was coated on the surface of AF through the polymerization reaction of dopamine, so that there were a large number of active groups on the surface of AF. After that, graphene oxide was fixed on the surface of AF by physical and chemical action by soaking graphene oxide solution, to obtain AF/PDA/GO. Fig. 2a is the electron microscope image of AF after cleaning without modification. It can be seen from the image that the surface of AF itself is smooth and composed of multiple strands of fibers. The surface roughness is low, resulting in poor bonding with the matrix. During the friction process, the matrix is easy to peel off, resulting in a large amount of friction and wear, reducing the service life of the parts. Fig. 2b is the AF electron microscope image after loading PDA [23,43]. The surface is loaded with a large number of polydopamine molecules, which can effectively increase the roughness of the AF surface and improve the combination of AF and EP. It has an effective effect on reducing the wear of the matrix during the friction process. At the same time, it has a positive effect on the loading of GO. It is difficult for flake GO to be directly loaded onto the AF surface. This situation can be improved by introducing PDA. Fig. 2c shows the surface of AF/PDA after the introduction of GO [44], and it can be observed that GO is loaded on the surface of the fiber.
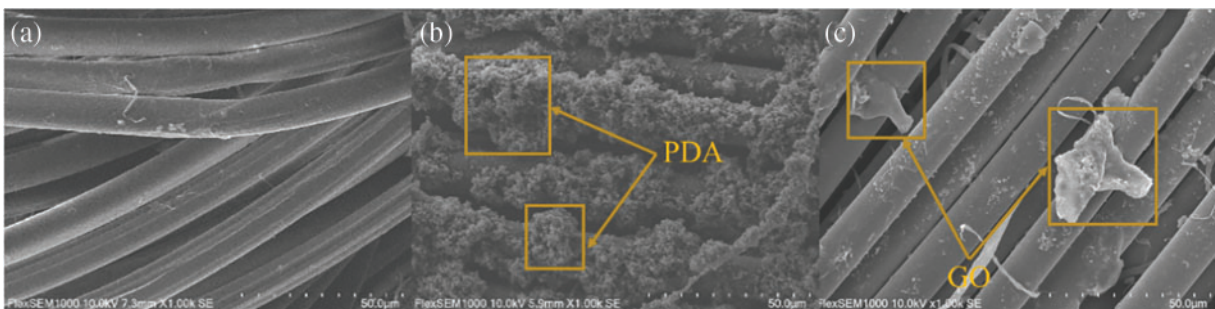

Figure 2: SEM of (a) AF, (b) AF/PDA, (c) AF/PDA/GO

The infrared spectra of EP and its composites are shown in Fig. 3a. It can be seen from the figure that the broad peak at 3300–3600 cm⁻¹ of pure epoxy resin is related to the-OH stretching vibration of EP. At 830 cm⁻¹, the C-O-C stretching vibration is the characteristic peak of the epoxy group [45], and the peaks at 2933 and 2852 cm⁻¹ are mainly C-H stretching vibration. The peaks at 1500 and 1600 cm⁻¹ are mainly the C=C stretching vibration of aromatic hydrocarbons [46]. The peaks at 1251, 1182, and

1045 cm^{-1} are mainly C-O stretching vibration. The peak at 553 cm^{-1} is an OH stretching vibration. Compared with pure EP, the modified matrix did not change significantly, which may be because the epoxy resin itself has a large number of epoxy groups, thus masking the characteristic peaks of the added modified substances. We conducted infrared tests on unpolished fibers and modified fibers, and the results are shown in Fig. 3b. The infrared characteristic peaks of aramid fiber are very similar to those of PDA and GO, which makes it difficult to distinguish the results.
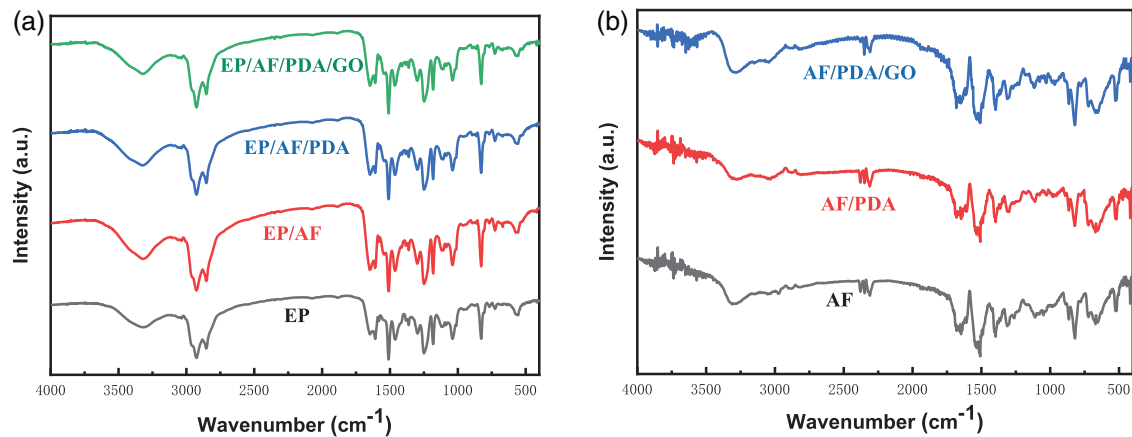

Figure 3: FTIR spectra of (a) EP, EP/AF, EP/AF/PDA and EP/AF/PDA/GO, (b) AF, AF/PDA and AF/PDA/GO

3.2 Mechanical Properties of EP and Its Composites

In order to explore the mechanical properties of the composite material, the surface hardness of the composite material was measured by a hardness tester, and the results were shown in Fig. 4. From the data of Fig. 4, the hardness of pure EP is about 56 SHD [23,47]. It can be seen that the hardness of the composite material increases slightly after adding AF, and the introduction of PDA and GO has no significant effect on the hardness of the composite material.
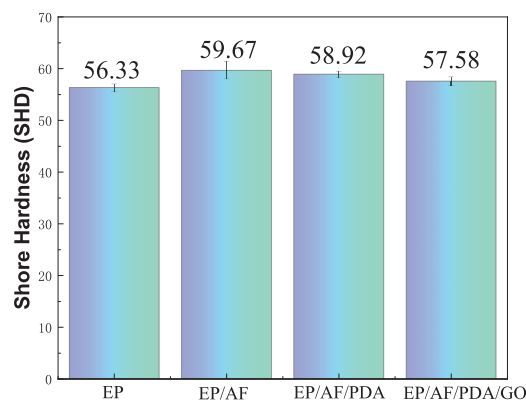

Figure 4: Hardness of EP, EP/AF, EP/AF/PDA and EP/AF/PDA/GO composite surfaces

In order to further explore, we conducted a tensile test on the composite material, and the experimental results are shown in Fig. 5a,b. Fig. 5a is the tensile strength and tensile modulus of the composite material. From the figure, it can be seen that after AF is added to the composite material, it's tensile strength and modulus are greatly improved [47,48]. The main reason is that AF has excellent mechanical properties, which can effectively prevent the direct fracture of the composite material

during the tensile process. After the introduction of PDA, GO, the tensile strength of the composites decreased slightly, but it was still higher than that of pure EP, and the tensile modulus decreased to some extent. Fig. 5b is the stress-strain curve of the composite material. The pure EP breaks directly during the tensile process. After adding AF, the mechanical properties of the composite material are greatly improved, which proves that AF plays a significant role in improving the mechanical properties of the composite material. However, the tensile strength and modulus of the composites decreased after the addition of PDA and GO, which needs further study.
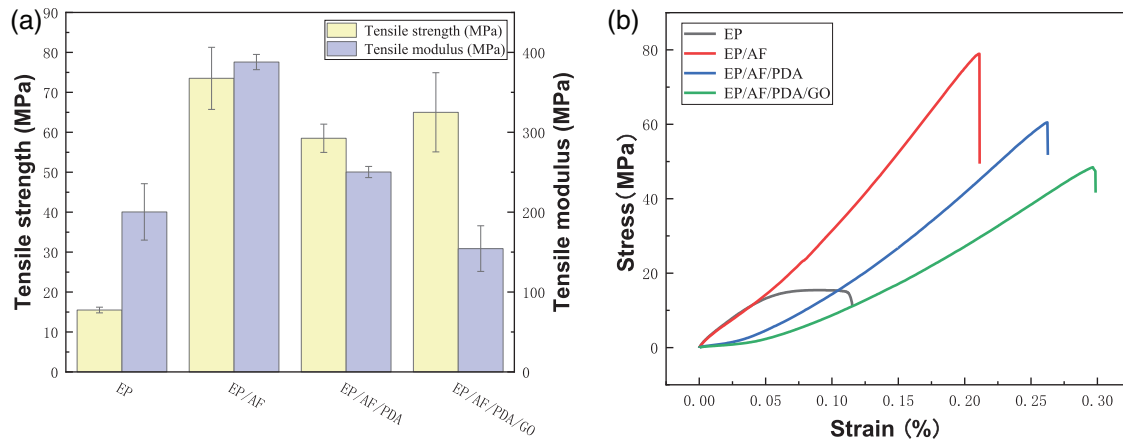

Figure 5: (a) Tensile strength and tensile modulus of different EP composites, (b) Stress-strain curve of different EP composites

3.3 Tribological Properties of EP and Its Composites

Fig. 6a is the change curve of friction coefficient with time of pure EP and modified composite under the condition of load 40 N and rotation speed 100 r/min. The friction coefficient of pure EP tends to be stable after the friction time reaches 300 s, and the friction coefficient is about 0.75 when it is stable [23,47]. After the introduction of woven AF as a support, the friction coefficient of EP/AF is lower than that of pure EP, but AF is difficult to play a good lubrication effect, so its friction coefficient is constantly fluctuating and growing, and it is difficult to achieve a stable friction stage. After the introduction of dopamine molecules, the components of the composite are tightly bonded. After 250 s of friction process, the friction coefficient reaches a stable state, about 0.50. Compared with pure EP, the friction coefficient is reduced to a certain extent, and the friction coefficient of EP/AF is basically the same. By introducing GO, the friction coefficient of the composite material has decreased significantly, reaching a stable friction state after 250 s, and the friction coefficient is about 0.42. It can be seen that GO, as a two-dimensional material, can play a certain role in reducing the friction coefficient of the composite material and can effectively reduce the friction coefficient of the composite material. Fig. 6b is specific wear rate and average friction coefficient of EP and its composites. It can be seen from the diagram that the friction coefficient and wear rate of the composite material decreased after the addition of AF. The friction coefficient and wear rate of the composite material after the addition of AF modified by PDA did not change significantly compared with EP/AF. However, after the introduction of GO, the friction coefficient and wear rate of the composite material were further reduced to achieve the best effect of the system. Compared with pure EP, the average friction coefficient is reduced by 48.36%, and the wear rate is reduced by 96.99%.
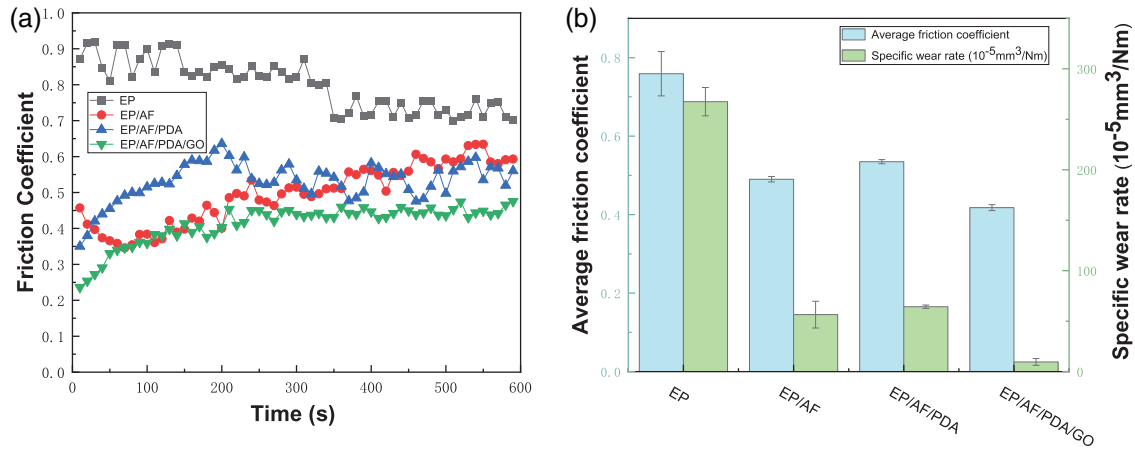
Figure 6: The tribological properties of EP and its composites: (a) coefficient of friction, (b) specific wear rate and average friction coefficient (40 N, 0.21 m/s)

3.4 Morphology of Wear Surface of EP and Its Composites

In order to study the tribological mechanism of pure EP and EP/AF/PDA/GO composites in detail, SEM images were taken at the wear scars of the corresponding composites. The results are shown in Fig. 7. Fig. 7a is the SEM image of the wear surface of pure EP. It can be seen that there are a large number of wear debris on the surface, as well as a large area of spalling due to friction [47]. After adding AF, it can be seen from Fig. 7b that the wear debris is reduced, and the wear surface becomes more flat. It can be seen that AF fiber has wear-resistant characteristics [49], and the wear debris on the wear surface is reduced. After the introduction of PDA, it can be seen from Fig. 7c that the peeling phenomenon of the matrix on the wear surface of the composite material is reduced, the fiber and the matrix are closely combined, and the amount of wear debris is further reduced compared with EP/AF. Fig. 7d is the wear surface of EP/AF/PDA/GO composites. It can be seen that the wear surface is smooth, and GO has a certain lubricating effect to fill the matrix wear caused by friction and wear. Compared with pure EP, the rough state of the friction surface is effectively improved.

In order to further explore the wear surface morphology of the composite material, the three-dimensional scanning of the wear surface was carried out [23]. The imaging results are as shown in Fig. 8. Fig. 8a shows the three-dimensional morphology of the wear scar surface of pure EP. It can be seen that the depth of the wear scar is deep, and there are a lot of wear debris generated by friction on the surface. Fig. 8b is the three-dimensional morphology of the wear scar surface of EP/AF, which is improved compared with pure EP, and the friction surface is relatively flat. After adding AF as a support, the wear depth is reduced. It can be seen that the addition of AF can improve the wear resistance of the composite material. Fig. 8c shows the wear scar surface of EP/AF/PDA. The wear scar is relatively shallow, and the friction surface is improved compared with EP/AF. The gully caused by surface friction is filled to a certain extent, it is proved that PDA can effectively improve the interfacial bonding between EP and AF in the composites, thus improving the tribological properties of the composites. Fig. 8d is the friction surface of EP/AF/PDA/GO composite material. The surface has a certain roughness, which may be that the GO sheet material plays a certain role on the friction surface.
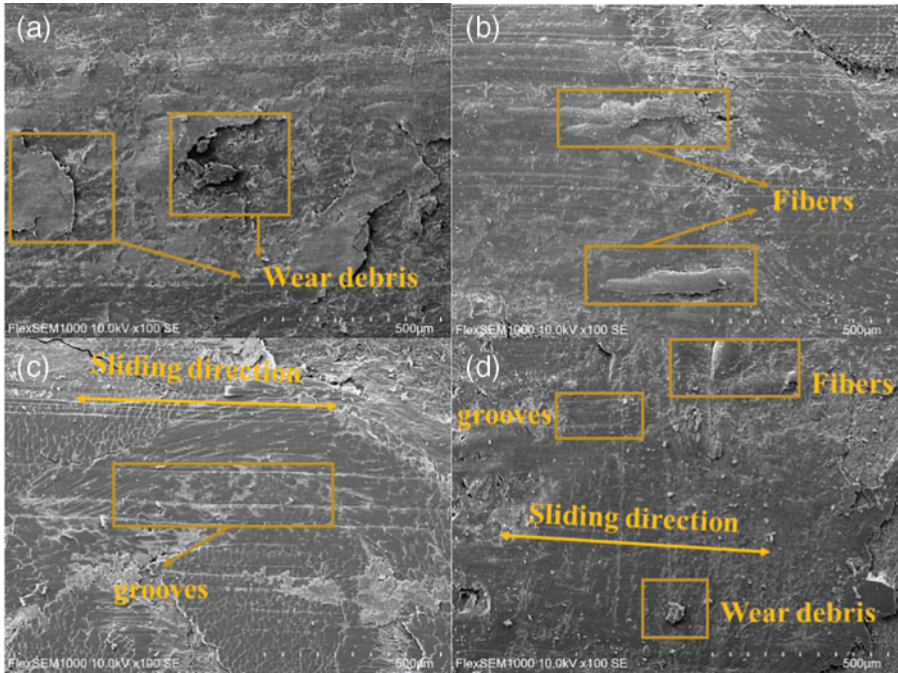
Figure 7: SEM of (a) EP, (b) EP/AF, (c) EP/AF/PDA, (d) EP/AF/PDA/GO worn-out surface
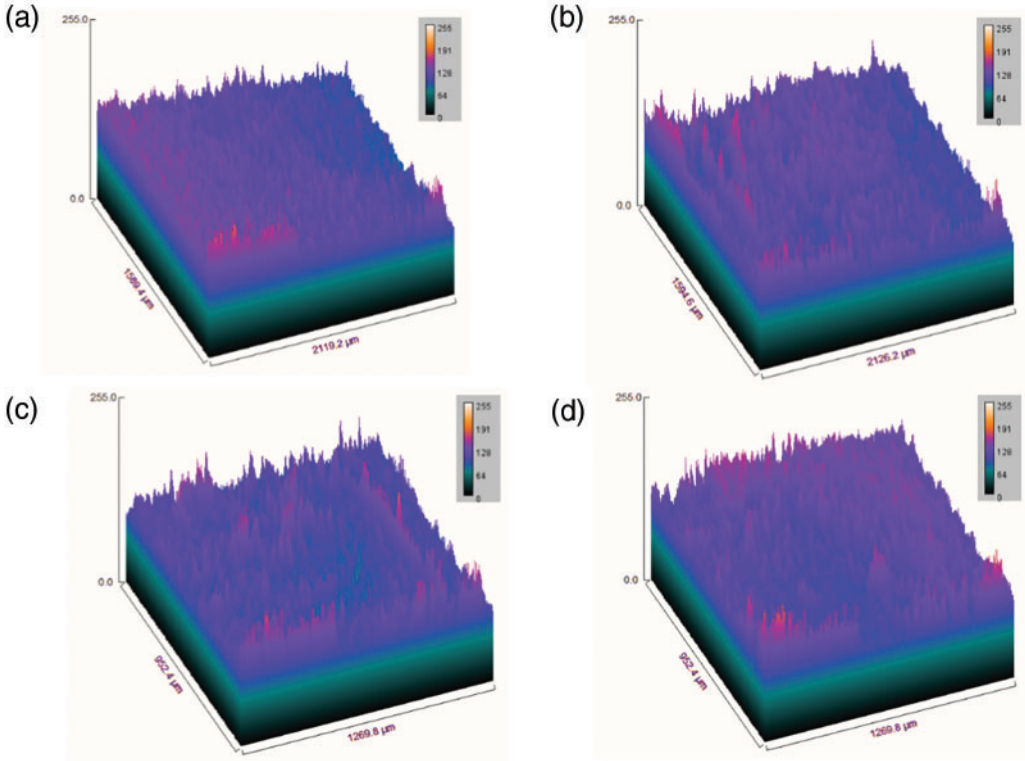

Figure 8: 3D profile of composite wear surface of (a) pure EP, (b) EP/AF, (c) EP/AF/PDA, (d) EP/AF/PDA/GO

Based on the above data, the tribological mechanism model diagram of EP and its composites is drawn in Fig. 9. It is speculated that the addition of AF fiber can reduce the wear rate of the composite material when the steel ring contacts with the composite material during the friction process. The GO loaded on the AF surface moves to the friction contact surface during the friction process, which plays a role in anti-friction and anti-wear. The GO synergistic with AF, filling the wear position of the friction surface, and reducing the wear of the composite material [44,50], so as to achieve good tribological properties. The results show that GO and AF play a great role in improving the tribological properties of EP composites.
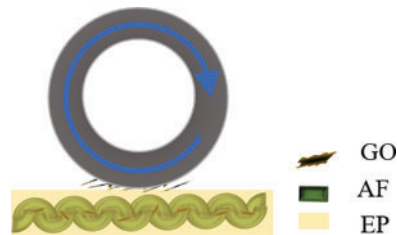

Figure 9: Schematic diagram of the friction reduction of EP composite

4 Conclusion

In this study, we weaved a single AF and then grafted a large number of active groups on the surface of the AF by coating a polydopamine coating on the braided fiber. GO is fixed on the surface of aramid fiber through the interaction with the active groups on the surface of aramid fiber, which plays a certain role in the friction process. It was found that the tribological properties of the EP/AF/PDA/GO composite have great improvement. Compared with pure EP, the friction coefficient is reduced by 48.36%, and the volume wear rate is reduced by 96.99%. The wear surface of the modified material has shallow wear marks, low roughness, and is relatively smooth. Also, we found that the introduction of AF greatly improves the mechanical properties of the composites. The addition of AF improved the hardness, tensile strength, and tensile modulus of the composites. In summary, AF/PDA/GO can be added into the matrix as a support to play a good anti-friction and wear-resistant effect.

Author Contributions: Study conception and design: Yuanyuan Feng, Bingli Pan; data collection: Xiaofan Ding, Xinyu Yuan; analysis and interpretation of results: Yuanyuan Feng, Yuxuan Zhou; draft manuscript preparation: Bingli Pan, Hongyu Liu. All authors reviewed the results and approved the final version of the manuscript.

Availability of Data and Materials: The datasets generated during and/or analyzed during the current study are available from the corresponding author on reasonable request.

Ethics Approval: Not applicable.

Conflicts of Interest: The authors declare that they have no conflicts of interest to report regarding the present study.

References

1. Liu H, Chen W, Yan Q, Chen Q, Hong M, Zhou Z-X, et al. Modified natural eucommia ulmoides gum effectively improves the toughness and strength of epoxy resins. ACS Appl Polym Mater. 2024;6(5):2567–75. doi:10.1021/acsapm.3c02720.
2. Ahrens A, Bonde A, Sun HW, Wittig NK, Hammershoj HCD, Batista GMF, et al. Catalytic disconnection of C-O bonds in epoxy resins and composites. Nature. 2023;617(7962):730–7. doi:10.1038/s41586-023-05944-6.
3. Shivakumar H, Gurumurthy GD, Bommegowda KB, Parameshwara S. Study of galvanic charging-discharging properties of graphene nanoplatelets incorporated epoxy-carbon fabric composites. J Polym Mater. 2023;40(1–2):93–103. doi:10.32381/JPM.2023.40.1-2.8.
4. Jeong H, Jang KS. Catalysis of silver and bismuth in various epoxy resins. Polymers. 2024;16(3):439. doi:10.3390/polym16030439.
5. Liu T, Zhao Y, Deng Y, Deng Y, Ge H. Preparation of fully epoxy resin microcapsules and their application in self-healing epoxy anti-corrosion coatings. Prog Org Coat. 2024;188(2):108247. doi:10.1016/j.porgcoat.2024.108247.
6. Zhao K, Hu ZJ, Wang BX, Li QH, Xu Y. Effect of roughness and adhesive on the strength of concrete-to-concrete interfaces cast from 3D-printed prefabricated plastic formworks. Constr Build Mater. 2023;368:130423.
7. Van Lijsebetten F, Maiheu T, Winne JM, Du Prez FE. Epoxy adhesives with reversible hardeners: controllable thermal debonding in bulk and at interfaces. Adv Mater. 2023;35(31):2300802.
8. Lei Z, Ma JW, Sun W, Yin B, Liew KM. Low-velocity impact and compression-after-impact behaviors of twill woven carbon fiber/glass fiber hybrid composite laminates with flame retardant epoxy resin. Compos Struct. 2023;321:117253.
9. Yin ZT, Wang BB, Tang QB, Lu JY, Liao C, Jia PF, et al. Inspired by placoid scale to fabricate MXene derivative biomimetic structure on the improvement of interfacial compatibility, mechanical property, and fire safety of epoxy nanocomposites. Chem Eng J. 2022;431:133489.
10. Meng FN, Zhang ZY, Gao PL, Kang RY, Boyjoo Y, Yu JH, et al. Excellent tribological properties of epoxy-Ti_3C_2 with three-dimensional nanosheets composites. Friction. 2021;9(4):734–46.
11. Zachariah SA, Shenoy S, Pai D. Experimental analysis of the effect of the woven aramid fabric on the strain to failure behavior of plain weaved carbon/aramid hybrid laminates. Facta Universit Series: Mech Eng. 2024;22(1):13–24. doi:10.22190/FUME200819022Z.
12. Lu GF, Liu HM, Qi XW, Dong Y, Fan BL, Zhang Y, et al. Multiscale insight to tribological mechanism of PTFE/aramid fiber composite liner containing PES/PMPS microcapsules under a high temperature environment. Tribol Int. 2024;192(1–2):109315. doi:10.1016/j.triboint.2024.109315.
13. Bin Manda MS, Rejab MRB, Abu Hassan S, Bin Wahit MU, Binoj JS, Mansingh BB, et al. Tin Slag polymer concrete strengthening by basalt and aramid fiber reinforced polymer confinement. J Polym Mater. 2022;39(3–4):241–53. doi:10.32381/JPM.2022.39.3-4.5.
14. Singh M, Dodla S, Gautam RK. Mechanical and tribological properties of CNTs coated aramid fiber-reinforced epoxy composites. Compos Part A: Appli Sci Manuf. 2024;179(3):108061. doi:10.1016/j.compositesa.2024.108061.
15. Tong YG, Wang L, Wang B, Hu YL, Cai ZH, Ren JN, et al. Microstructure and mechanical behavior of carbon fiber reinforced carbon, silicon carbide, and copper alloy hybrid composite fabricated by Cu-Si alloy melt infiltration. Adv Compos Hybrid Mater. 2023;6(1):25. doi:10.1007/s42114-022-00612-1.
16. Ma SS, Li HJ, Fei J, Li C. Flexible-rigid scalable structures for trans-scale interface reinforcement of carbon fiber/phenolic composites: effect on properties. Compos Part B: Eng. 2023;258:110703.
17. Mao LH, Jiao YA, Geng HH, Tang YH. Understanding friction and wear properties of carbon fiber/epoxy stitched composites. Compos Part A: Appl Sci Manuf. 2023;169:107501.

18. Chen JX, Zhou L, Zhu ZM, Ma LJ, Wang M, Deng Z. Crack propagation analysis and mechanical properties of basalt fiber reinforced cement composites with changing fiber surface characteristics. Constr Build Mater. 2023;392:131738.

19. Wang FF, Wang JJ, Fang D, Zhou SF, Huang J, Zhao GZ, et al. Surface sizing introducing carbon nanotubes for interfacial bond strengthening of basalt fiber-reinforced polymer composites. Adv Compos Hybrid Mater. 2023;6(3):117.

20. Huang Y, Cai M, He C, Si CY, Li L, Fan XQ, et al. Basalt fiber as a skeleton to enhance the multi-conditional tribological properties of epoxy coating. Tribol Int. 2023;183:108390.

21. Rubio-Aguinaga A, Reglero-Ruiz JA, García-Gómez A, Martín EP, Ando S, Muñoz A, et al. Boron nitride-reinforced porous aramid composites with enhanced mechanical performance and thermal conductivity. Compos Sci Technol. 2023;242:110211. doi:10.1016/j.compscitech.2023.110211.

22. Lertwassana W, Parnklang T, Mora P, Jubsilp C, Rimdusit S. High performance aramid pulp/carbon fiber-reinforced polybenzoxazine composites as friction materials. Compos Part B: Eng. 2019;177(9):107280. doi:10.1016/j.compositesb.2019.107280.

23. Zhou YX, Pan BL, Wang MD, Feng YY, Nie PP, He XJ. Tribological properties of differently shaped zinc-based metal-organic framework particles reinforced epoxy resin composites. J Appl Polym Sci. 2023;140(48):e54738. doi:10.1002/app.54738.

24. Seyedin S, Uzun S, Levitt A, Anasori B, Dion G, Gogotsi Y, et al. MXene composite and coaxial fibers with high stretchability and conductivity for wearable strain sensing textiles. Adv Funct Mater. 2020;30(12):1910504. doi:10.1002/adfm.201910504.

25. Song LM, Wu CW, Zhi Q, Zhang F, Song BZ, Guan L, et al. Multifunctional SiC aerogel rein-forced with nanofibers and nanowires for high-efficiency electromagnetic wave absorption. Chem Eng J. 2023;467(3):143518. doi:10.1016/j.cej.2023.143518.

26. Rodríguez-Fabia S, Zarna C, Chinga-Carrasco G. A comparative study of kraft pulp fibres and the corresponding fibrillated materials as reinforcement of LDPE- and HDPE-biocomposites. Compos Part A: Appl Sci Manuf. 2023;173(5):107678. doi:10.1016/j.compositesa.2023.107678.

27. Lv Y, Xu XH, Tang W, Peng YQ, Yang JM. Interface design and mechanical performance evaluation of MKPC-based materials reinforced with fibreglass spacer fabric. Case Stud Constr Mater. 2023;19(7):e02511. doi:10.1016/j.cscm.2023.e02511.

28. Chen Y, Du B, Xue R, Xing Y, Kong X. Polydopamine-enabled surface modification to improve the dielec-tric property of aramid fiber/epoxy composites for insulation rod. ACS Appl Polym Mater. 2024;6(13):7524–31. doi:10.1021/acsapm.4c00914.

29. Lin J, Du YL, Ma XX, Li Y, Xie YT, Qi HD, et al. Choline chloride/urea etched carbon fiber to improve the elasticity of biomass-based carbon aerogel for efficient oil-water separation. Colloids Surf A: Physicochem Eng Asp. 2023;669(2):131506. doi:10.1016/j.colsurfa.2023.131506.

30. Li Y, Sun SY, Zhou Y, Xu XF, Zhan JC. Influence of air plasma modification power on surface properties of basalt fibers and basalt/poly(butylene succinate) adhesion. Appl Surf Sci. 2023;630:157416. doi:10.1016/j.apsusc.2023.157416.

31. Gapsari F, Darmadi DB, Juliano H, Hidayatullah S, Suteja, Rangappa SM, et al. Modification of palm fiber with chitosan-AESO blend coating. Int J Biol Macromol. 2023;242:125099.

32. Salman MS, Sheikh MC, Hasan MM, Hasan MN, Kubra KT, Rehan AI, et al. Chitosan-coated cotton fiber composite for efficient toxic dye encapsulation from aqueous media. Appl Surf Sci. 2023;622:157008.

33. Xu ZC, Sun HY, Huo YL, Jia MJ, Chen ZT, Yang YZ. $Ti_3C_2T_x$ MXene modified polyethylene fibers for enhancing interface properties of strain-hardening cementitious composites. Cem Concr Compos. 2024;145:105358.

34. Sun N, Zhu B, Gao XP, Qiao K, Zhang Y, Wang BM, et al. Improved the interfacial characteristics of carbon fiber/polyamide 6 composites by synthesizing polydopamine rapidly on the carbon fiber surface with ultrasound-assisted. Compos Sci Technol. 2023;234:109950.

35. Somberg J, Gonçalves G, Emami N. Graphene oxide versus graphite and chemically expanded graphite as solid lubricant in ultrahigh molecular weight polyethylene composites. Tribol Int. 2023;187:108643.

36. Liu HY, Fan XB, Pan BL, Zhou YX, Zhang LL, Li MH, et al. Simultaneously enhancing tribological and mechanical properties of epoxy composites using basalt fiber/reduced graphene oxide/paraffin wax. Polym Compos. 2024;45(4):3343–54. doi:10.1002/pc.27994.

37. Hu WL, Cheng WC, Wang YH, Wen SJ. Feasibility study of applying a graphene oxide-alginate composite hydrogel to electrokinetic remediation of Cu(II)-contaminated loess as electrodes. Sep Purif Technol. 2023;322(16):124361. doi:10.1016/j.seppur.2023.124361.

38. Wang LP, Pan BL, Gao JY, Huang SS, Xie MX, Li CY, et al. Tribological behaviors of porous 3D graphene lubricant reinforced monomer casting polyamide 6 composite. Adv Eng Mater. 2020;22(5):1901170. doi:10.1002/adem.201901170.

39. Fan XQ, Zhao Z, Li CD, Li XR, He YS, Zhu MH. Deep eutectic solvent intercalation graphene oxide with strong interfacial adsorption capacity towards efficient lubrication. Carbon. 2024;216(1):118508. doi:10.1016/j.carbon.2023.118508.

40. Feng JG, Safaei B, Qin ZY, Chu FL, Scarpa F. Bio-inspired metallic cellular material with extraordinary energy dissipation capability. Chem Eng J. 2023;475:146382. doi:10.1016/j.cej.2023.146382.

41. Wang JJ, Zhou SF, Huang J, Zhao GZ, Liu YQ. Interfacial modification of basalt fiber filling composites with graphene oxide and polydopamine for enhanced mechanical and tribological properties. RSC Adv. 2018;8(22):12222–31. doi:10.1039/C8RA00106E.

42. Marcano DC, Kosynkin DV, Berlin JM, Sinitskii A, Sun Z, Slesarev A, et al. Improved synthesis of graphene oxide. ACS Nano. 2010;4(8):4806–14. doi:10.1021/nn1006368.

43. Qin WZ, Lei KX, Yan ML, Li ZK, Yan Y, Hu YW, et al. Carbon fiber-reinforced epoxy composite properties improvement by incorporation of polydopamine sizing at fiber-matrix interface. Polym Compos. 2023;44(4):2441–8. doi:10.1002/pc.27255.

44. Huang SS, Pan BL, Xie MX, Gao JY, Zhao GM, Niu YM, et al. Synergistic effects of graphene oxide and paraffin wax on the tribological properties of monomer casting nylon-6 composites. Tribol Int. 2021;154:106726. doi:10.1016/j.triboint.2020.106726.

45. Wu BR, Cui X, Jiang HY, Wu N, Peng CY, Hu ZF, et al. A superhydrophobic coating harvesting mechanical robustness, passive anti-icing and active de-icing performances. J Colloid Interface Sci. 2021;590:301–10. doi:10.1016/j.jcis.2021.01.054.

46. Cheng Z, Zhang LJ, Jiang C, Dai Y, Meng CB, Luo LB, et al. Aramid fiber with excellent interfacial properties suitable for resin composite in a wide polarity range. Chem Eng J. 2018;347:483–92.

47. Li Y, Zhou Y, Wang Y, Liu M, Yuan J, Men X. Facile synthesis of $WS_2@$ GO nanohybrids for significant improvement in mechanical and tribological performance of EP composites. Tribol Int. 2021;163:107148.

48. Savotchenko S, Kovaleva E. Mechanical properties of cured epoxy resin. Mod Phys Lett B. 2021;35:2150445.

49. Jing WW, Zhang F, Chen H. Comparative tribological performance and erosion resistance of epoxy resin composite coatings reinforced with aramid fiber and carbon fiber. Colloids Surf A: Physicochem Eng Asp. 2022;648:129354.

50. Liu HY, Wang Z, Pan BL, Li MH, Huang SS, Lee JH, et al. Carbon felt/nitrogen-doped graphene/paraffin wax 3D skeleton regulated tribological performances of the MCPA6 composites: a novel strategy of oil embedding and transporting. Tribol Int. 2023;184:108440.